Article
Chinese Science Bulletin
Geology
January 2011 Vol.56 No.3: 306–318
doi: 10.1007/s11434-010-4236-7

# Discovery of Paleoproterozoic rapakivi granite on the northern margin of the Yangtze block and its geological significance

ZHANG LiJuan[1], MA ChangQian[1,2*], WANG LianXun[1], SHE ZhenBing[1] & WANG ShiMing[1]

[1] *Faculty of Earth Sciences, China University of Geosciences, Wuhan 430074, China;*
[2] *State Key Laboratory of Geological Processes and Mineral Resources, CUG, Wuhan 430074, China*

Received September 3, 2010; accepted September 30, 2010

The Huashanguan rapakivi pluton in Zhongxiang, Hubei Province, China, is the first discovered Proterozoic rapakivi pluton in the Yangtze block. Based on field and petrographical observations, a typical rapakivi texture was found in the northern portion of the Huashanguan granitic pluton. Almost all the K-feldspar phenocrysts were round to oval in shape and most had plagioclase coatings known as rapakivi phenocrysts. Alkali feldspars and quartz had two or more generations. Petrochemically, the Huashanguan rapakivi granites were characterized as having high values of Si, K, Fe, Th, U, La, Ga, Ce, Sm and LREE, low values of Ca, Mg, Sr, Nb, Y and HREE, and a negative Eu anomaly. These geochemical characteristics of the Huashanguan granites were concordant with typical rapakivi granites, and had an affinity to A-type granites. LA-ICP-MS U-Pb zircon dating also was conducted. The dating yielded a $^{207}Pb/^{206}Pb$ weighted mean age of 1851±18 Ma (MSWD =1.2), which represents the age of the pluton emplacement. The age of 803±170 Ma at the lower intercept in the concordia diagram corresponds to the age of a later deformation event which affected the pluton, and suggests that the Huashanguan pluton was influenced by Neoproterozoic thermo-tectonic events after its formation. The discovery of Paleoproterozoic Huashanguan rapakivi granites indicates continental rifting or a post-orogenic extensional event that took place in the Paleoproterozoic in the Yangtze block. These events may be related to the breakup of the Paleoproterozoic Columbia supercontinent.

**Yangtze block, rapakivi, Paleoproterozoic, A-type granite, zircon U-Pb dating**

**Citation:** Zhang L J, Ma C Q, Wang L X, et al. Discovery of Paleoproterozoic rapakivi granite on the northern margin of the Yangtze block and its geological significance. Chinese Sci Bull, 2011, 56: 306–318, doi: 10.1007/s11434-010-4236-7

Rapakivi granite is a special rock type (typical A-type granite) in the crust that shows rapakivi texture [1]. Rapakivi granites are indicative of large-scale extensional tectonic settings, and usually are associated with the breakup of a supercontinent [1–7]. Rapakivi granites are exposed on the interiors and edges of all Proterozoic cratons worldwide, especially in the Northern Hemisphere. They form a near east-west giant rapakivi granite-anorthosite belt, which extends from the southwest of North America to the North China Platform, via Labrador in Canada, South Greenland, the Baltic Shield and the Sciberian Platform [1–8]. The origin of the belt is considered to be related to the breakup of the Columbia supercontinent [9–14]. Thus, rapakivi granites are important for understanding the evolution of the Proterozoic lithosphere.

The North China block and the Yangtze block are the two largest Precambrian cratons in China. Archean rocks are widely exposed in the North China block, and there are many records of the Proterozoic tectonothermal events related to the amalgamation and breakup of the Columbia supercontinent [10,15–24], including the Miyun Proterozoic typical rapakivi granites in Beijing [5–7,10]. However, outcrops of Archean basement rocks (e.g. Kongling Complex) are rare in the Yangtze block [25–28]. Even so, recent studies have shown that there are chronological records of 1.8–2.1Ga tectonothermal events in the Yangtze block [29–38]. Some of these studies indicates that these events may be related to the amalgamation and breakup of the Columbia

*Corresponding author (email: cqma@cug.edu.cn)

supercontinent [34–38]. However, there have been no reports of any Paleoproterozoic rapakivi granites within the Yangtze block. Thus, in this paper, we present the newly identified Huashanguan rapakivi granitic pluton in Zhongxiang, Hubei Province. In addition, we provide a study of petrography, LA-ICP-MS zircon U-Pb geochronology, and major and trace element geochemistry and discuss the significance of the discovery for understanding Paleoproterozoic crustal evolution of the Yangtze block.

## 1 Regional geological setting and intrusive geology

Huashanguan granitic intrusions are, with the total area of 37 km$^2$, located in Zhongxiang, Hubei Province, on the northern margin of the Yangtze block (Figure 1). The intrusions consist of four granitic bodies of variable sizes. They are the Huashanguan, Wangjiapeng, Huachong and Xiaojiawan intrusions, and their areas are 22, 12, 2 and 1 km$^2$, respectively. And the intrusions are distributed nearly north-south in the core of an anticline and secondary small anticline in Lengshui town. According to the survey of regional geology [39], the pluton intruded into the Paleoproterozoic Yangpo Formation, equivalent to the upper lithologic formation of the Archean Kongling Complex. Thus, the contact between the intrusions and the overlying Nanhua-Sinian strata is an unconformity, and xenoliths from the Yangpo Formation are visible in the pluton. The main rock types of the Huashanguan and Wangjiapeng intrusions are porphyraceous syenogranite and medium grained biotite adamellite with a few feldspar phenocrysts, and there is a gradual transition between the two rock types. While there is only medium grained biotite adamellite in the Huachong intrusion, and that of the Xiaojiawan intrusion is only porphyraceous syenogranite. Xenoliths with schist, gneiss and plagioclase amphibolite remnants also can be seen in the four intrusive bodies. As a result of dynamic metamorphism, the intrusions and the country rocks suffered a certain degree of deformation[1)].

The rapakivi granites reported in this paper are exposed in the porphyraceous syenogranite unit in the northern portion of the Huashanguan pluton. The sample used for zircon dating was collected at 31°17.261′N, 112°24.607′E (Figure 1(b). The rock had a porphyraceous texture, and the matrix was medium to coarse grained. The phenocryst was a microcline perthite with a plagioclase rim, and the matrix was microcline perthite, quartz, plagioclase, biotite and other components. The main mineral components were: microcline perthite 65%, plagioclase 10% (mostly changed to sericite), quartz 23%, and biotite 2%. As the scale of the Huashanguan rapakivi granites was limited (<1 km$^2$), we only collected two samples (ZX21-1 and 09ZX03) for analysis. For comparison, we also collected a porphyritic biotite adamellite sample (09ZX01-1) near the Huashanguan rapakivi granite pluton. The porphyritic biotite adamellite

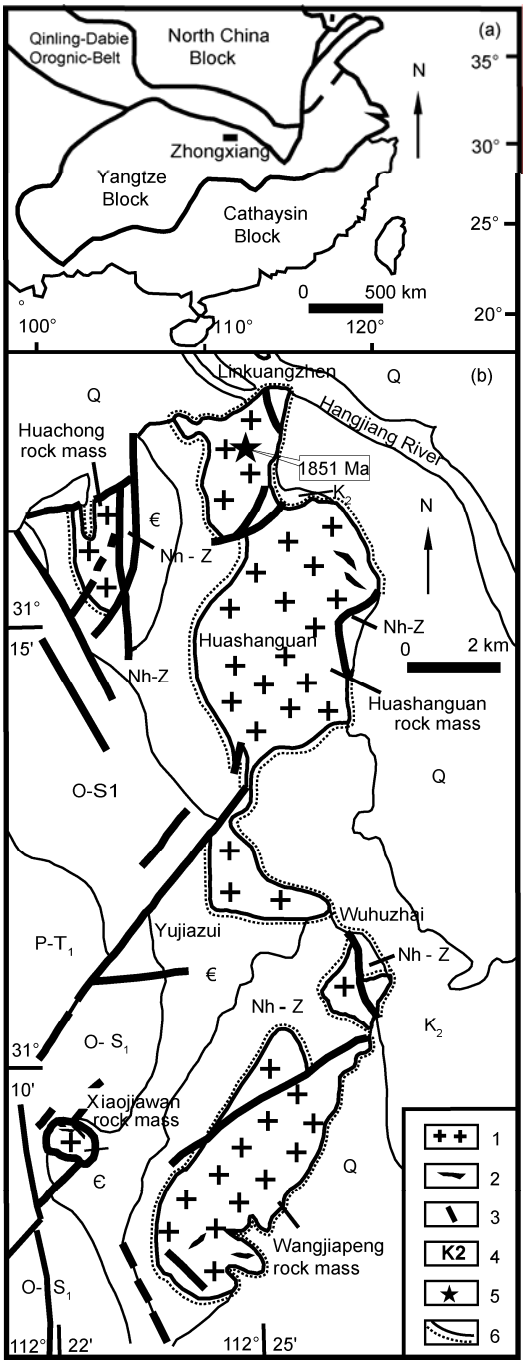


**Figure 1** Geological map of Huashanguan area rock mass. 1, Porphyraccous syenogranite and medium grained biotite adamellite; 2, basic dikes; 3, faults: 4, sedimentary strata (Nh-Z: Nahuaian-Sinian; Є: Cambrian; O-Si: Ordovician-Lower Silurian; $K_2$: Upper Cretaceous; P-$T_1$: Permian-Lower Triassic; Q: Quatemary); 5, collection site of zircon dating sample; 6, unconformaity boundary. (a) is modified from [36]; (b) is a modified drawing based on the 1:200000 geological map of the Zhongxiang area, drawn by the Survey Geological Team of the Hubei Provincial Geological Bureau.

1) Modified from reports of the 1:200000 regional geological survey of Zhongxiang and the 1:50000 regional geological survey of Shu anghekou, Hubei Province.

was medium grained, and had a few phenocrysts. The main minerals were: microcline perthite 49%, plagioclase 27%, quartz 22%, and biotite 2%.

## 2 Rapakivi texture and its petrography

The rapakivi texture was first introduced into the international geological literature in 1980 by Jakob J. Sederholm, a famous Finnish geologist [40]. The name "rapakivi granite" is derived from the Finnish word "rapakivi", which means "crumbly rock" and refers to the distinctive weathering behaviour. The Huashanguan rocks with rapakivi textures are grey white to flesh red with porphyraceous textures. These granites are characterized by the ovoidal shape of their alkali feldspar megacrysts, mantling of many ovoids by oligoclase-andesine shells, and some the ovoids remaining unmantled. The ovoids show two generations of alkali feldspar and quartz, which is consistent with the definition of rapakivi granites [1–3,6,7]. These characteristics show that Huashanguan rocks with rapakivi textures belong to typical rapakivi granites. The diameter of the ovoids generally was between 1 cm and 5 cm, with some individuals were over 8 cm, but the most common size range was 2–3 cm (Figure 2). The percent volume of alkali feldspar phenocrysts accounted for about 45% of the rock. Most of the phenocrysts consist of 3–5 K-feldspar crystals (Kfs), whose optical orientation differed and the single particle size is 5–10 mm with a flabellate shape. They grew poikiliticly to ovoid shape, from the core outward to the rims (Figure 3(a)). Few of the phenocrysts consisted of single K-feldspar crystals. Plagioclase (pl), quartz (Qtz), biotite (Bi), magnetite (Mt) and other small crystals often were wrapped in the ovoidal K-feldspar phenocrysts. These minerals were embedded unevenly in the host crystal (Figure 3(b)), and showed a tendency toward sphericity. Between the joint surface of the fan-shaped K-feldspar crystals, there were vein fillings of biotite, magnetite, quartz and others (Figure 3(a)). Perthitic structure and cross hatched twins were developed in K-feldspar phenocrysts, which belonged to microcline perthite. Most K-feldspar and quartz coexisted, and some showed micrographic textures (Figure 3(c)). Matrix compositions mainly were alkali feldspar, plagioclase, quartz and biotite. Alkali feldspar and quartz could be divided clearly into two or more generations. The particles of early crystallization were larger, and the later generation crystals were smaller. Figure 3(d) indicates that the quartz sizes were significantly different, and the larger crystals were mostly rounded. Accessory minerals mainly were fluorite, apatite, magnetite, and zircon. These features were similar to that of typical Proterozoic rapakivi granites from Finland, Miyun (Beijing) and other places [1–10,41,42].

During dynamic metamorphism, most of the rocks suffered from deformation and alteration to different degrees. A few of biotite changed to chlorite, and plagioclase mostly changed to sericite. In the deformation zone, wavy extinctions of quartz, kink deformation of biotite, and brittle fractures and intragranular changes of feldspar were obvious (Figure 3(d)–(f)).

## 3 Analytical methods

Samples for major and trace element analyses were crushed to less than 200 microns. The analysis of major elements was conducted with X-ray fluorescence spectrometry (XRF) with a Regaku3080E1-type spectrometer at the Geological Experiment Center of Hubei Province. The accuracy of the sample analysis was 1% [43]. Trace elements were analyzed with an inductively coupled plasma mass spectrometer (ICP-MS, Agilent7500a) at the State Key Laboratory of Geological Processes and Mineral Resources in China University of Geosciences (Wuhan). The accuracy of the rare earth element analyses was higher than 5%, and the analytical precision of the other trace elements was 5% to 15%. Details of the analytical methods and apparatus are reported in a previous literature report [44]. The zircons in sample ZX21-1 were separated by standard heavy mineral separation

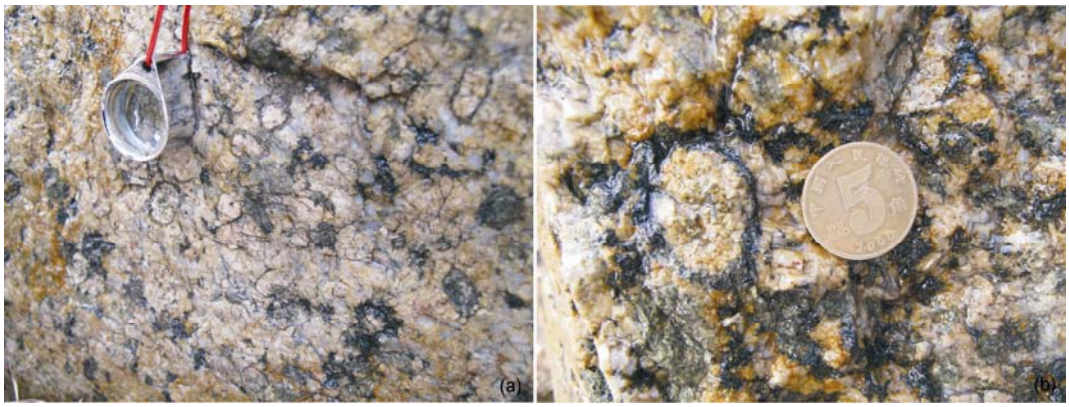


**Figure 2** Field photographs of Huashanguan rapakivi granites. (a) and (b) reveal that the K-feldspar ovoids are rimmed by the plagioclase.

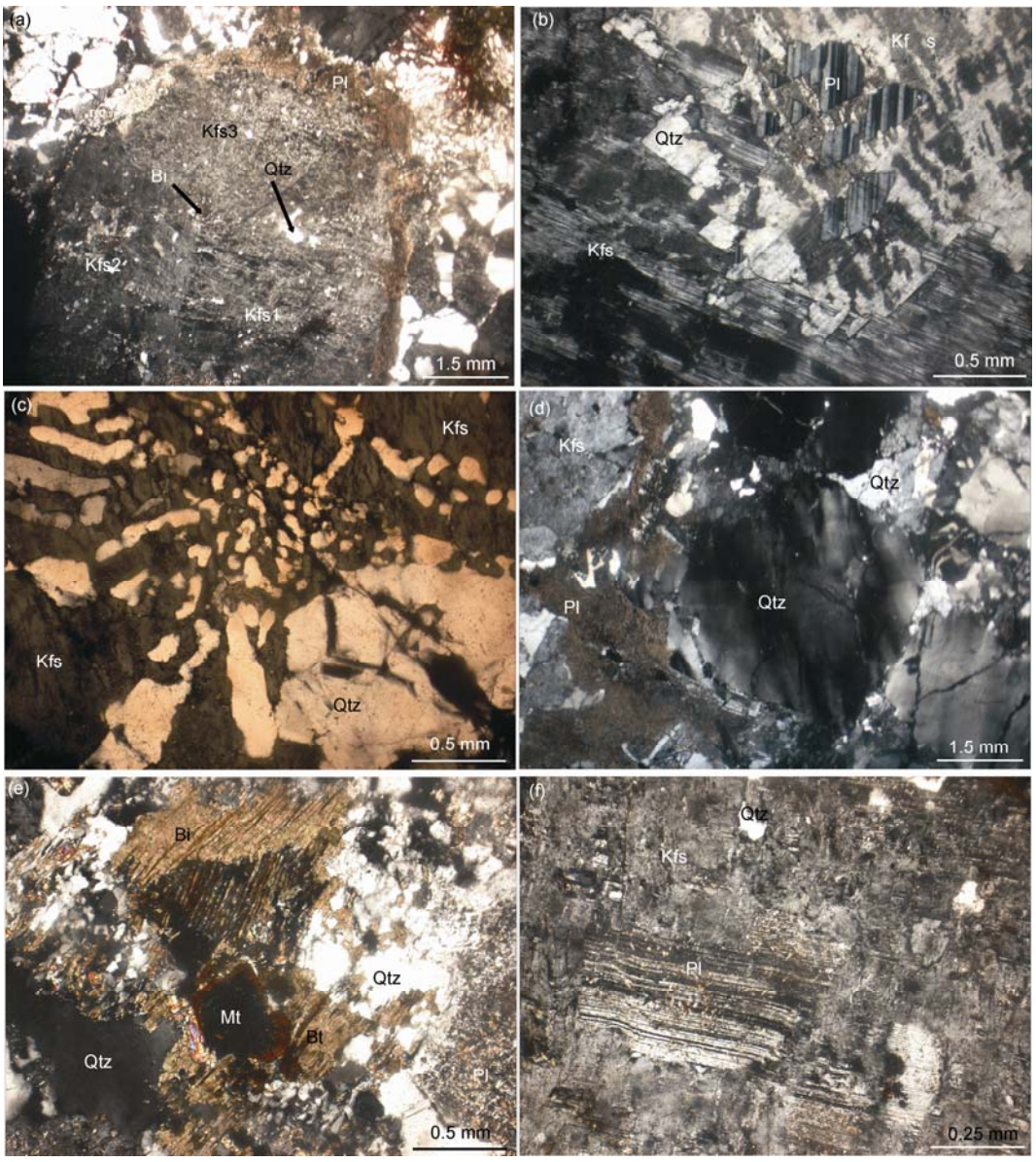


**Figure 3** Photomicrographs of Huashanguan rapakivi granites (orthogonal). (a) Phenocrysts consist of three K-feldspar crystals (Kfs1–3), with different light crystal orientations, and the shapes are flabellate. They grew poikilitic ly from the core outward to the rim to ovoid shape. The outside of the phenocrysts was characterized by plagioclase (Pl) shells (sericite). (b) K-feldspar (Kfs) ovoid example with plagioclase (Pl) and quartz (Qtz) within. Plagioclase (pl) and quartz (Qtz) are wrapped in an ovoid K-feldspar phenocryst. (c) Microscopic structure of K-feldspar (Kfs) and quartz (Qtz) in a phenocryst. (d) Rounded quartz (Qtz) and its wavy extinction in the matrix. (e) Kink deformation of biotite (Bi) in the matrix. (f) Kink deformation of plagioclase (Pl) twins in the matrix.

techniques, including magnetic and heavy liquid separation. Then, representative zircon grains, transparent and no cracks, were selected and imbedded into epoxy resin sample targets under a binocular microscope. The samples were polished after grinding to the center of the zircon particles, and then Cathodoluminescence (CL) microstructures were observed. On that basis, suitable particles and regions for zircon U-Pb age determination were selected. Zircon CL imaging were done using a Hitachi S3000-N scanning electron microscope, equipped with external Chroma cathodoluminescence made in the GATAN company at the Beijing SHRIMP Centre. Micro-area analysis of zircon for U-Pb isotopic and REE composition analyses was completed using an LA-ICP-MS at the State Key Laboratory of Geological Processes and Mineral Resources in China University of Geosciences (Wuhan). The laser ablation system was a GeoLas 2005 equipped with a 193-nm laser. The spot size of the laser was 32 μm, and the pulse was 10 Hz, with energy of 110 mJ. The ICP-MS was an Agilent7500a, which was produced by the Agilent Company, United States. We used helium as the carrier gas of the erosion material in the experiment, zircon 91500 as external standard for isotope

component corrections, and we calibrated elemental content with an NIST610 as the external standard and $^{29}Si$ as the internal standard. The original data were analyzed with ICPMSDATACAL (ver 5.8) software processing [45]. Common lead was corrected with the method of Andersen [46]. The weighted mean age of the zircons and the calculation of concordia diagrams were undertaken using the ISOPLOT_3.23 process [47].

## 4 Results

### 4.1 Major and trace elements

The major and trace elemental analyses of the Huashanguan rapakivi granites (sample ZX21-1 and 09ZX03) and porphyritic biotite adamellite (sample 09ZX01-1) are listed in Table 1.

As can be seen from Table 1, the Huashanguan rapakivi granites were rich in silicon ($SiO_2$= 69.92%–74.42%), alkali ($Na_2O$ + $K_2O$ = 8.84%–9.23%), potassium ($K_2O/Na_2O$ = 1.92%–2.52%) and iron (FeO*/(FeO*+ MgO) = 0.876%–0.88%) (FeO* is total iron), and poor in calcium (CaO = 0.22%–1.15%) and magnesium (MgO=0.21%–0.42%). The Al saturation index (A/CNK was close to 1.1, which places the study samples into the category of peraluminous rock. The Miyun rapakivi granites were metaluminous to peraluminous, and the A/CNK of Huashanguan porphyritic biotite adamellite equaled 1. All samples were within the composition region of the Finnish typical rapakivi granites (Figure 4(a)). The FeO*/(FeO*+MgO)-$SiO_2$ diagram (Figure 4(b)) shows that the Huashanguan rapakivi granites had high Fe/Mg ratios, which is similar to that of Miyun typical rapakivi granites, and both of the sample sets fall into the Finnish typical rapakivi granite compositional area. Conversely, the Fe/Mg ratio of Huashanguan porphyritic biotite adamellite was relatively lower, outside the Finnish region.

The Ce contents of the Huashanguan rapakivi granites were 123–256 μg $g^{-1}$, Ga was 19.1–23 μg $g^{-1}$, 10000 Ga/Al was 2.8–3.0, and $(La/Sm)_N$ was greater than 5.76, which belonged

**Table 1** The major (%) and trace element (μg $g^{-1}$) compositions of Huashanguan rapakivi granites and porphyritic biotite adamellite and related parameters

| Sample | ZX21-1 | 09ZX01-1 | 09ZX03 | Sample | ZX21-1 | 09ZX01-1 | 09ZX03 |
|---|---|---|---|---|---|---|---|
| $SiO_2$ | 69.92 | 75.48 | 74.42 | Er | 6.32 | 7.66 | 2.68 |
| $TiO_2$ | 0.45 | 0.17 | 0.38 | Tm | 0.87 | 1.14 | 0.43 |
| $Al_2O_3$ | 14.50 | 12.35 | 13.02 | Yb | 5.69 | 7.99 | 3.05 |
| $Fe_2O_3$ | 2.06 | 1.12 | 1.31 | Lu | 0.83 | 1.16 | 0.48 |
| FeO | 1.25 | 0.70 | 0.30 | ΣREE | 676.38 | 762.36 | 268.29 |
| MnO | 0.03 | 0.01 | 0.01 | δEu | 0.35 | 0.07 | 0.63 |
| MgO | 0.42 | 0.13 | 0.21 | Li | 6.89 | 5.23 | 4.94 |
| CaO | 1.15 | 0.89 | 0.22 | Be | 5.31 | 3.24 | 2.88 |
| $Na_2O$ | 3.03 | 2.95 | 2.62 | Sc | 6.99 | 2.49 | 4.42 |
| $K_2O$ | 5.81 | 5.43 | 6.61 | V | 15.70 | 1.90 | 11.90 |
| $P_2O_5$ | 0.07 | <0.01 | 0.03 | Cr | 3.18 | 2.08 | 3.05 |
| $H_2O^+$ | 0.97 | 0.48 | 0.61 | Co | 3.07 | 0.94 | 0.57 |
| $CO_2$ | 0.13 | 0.16 | 0.02 | Ni | 2.48 | 1.70 | 1.53 |
| LOI | | 0.87 | 0.62 | Cu | 6.27 | 3.46 | 6.41 |
| Total | 99.79 | 100.74 | 100.38 | Zn | 67.40 | 24.00 | 14.8 |
| A/CNK | 1.085 | 1.00 | 1.097 | Ga | 23.00 | 22.20 | 19.10 |
| $K_2O/Na_2O$ | 1.92 | 1.84 | 2.52 | Rb | 294.00 | 458.00 | 249.00 |
| FeO*/MgO | 7.39 | 13.14 | 7.04 | Sr | 132.00 | 27.60 | 140.00 |
| $K_2O+Na_2O$ | 8.84 | 8.38 | 9.23 | Y | 69.5 | 80.80 | 22.00 |
| La | 183.00 | 190.00 | 63.00 | Zr | 467.00 | 254.00 | 397.00 |
| Ce | 256.00 | 351.00 | 123.00 | Nb | 33.00 | 49.60 | 25.90 |
| Pr | 40.50 | 38.80 | 13.20 | Cs | 2.61 | 1.82 | 0.90 |
| Nd | 129.00 | 115.00 | 44.50 | Ba | 915.00 | 86.20 | 1228.00 |
| Sm | 20.00 | 18.00 | 6.66 | Hf | 14.00 | 9.69 | 11.30 |
| Eu | 2.11 | 0.39 | 1.19 | Ta | 2.03 | 3.89 | 1.80 |
| Gd | 15.40 | 13.90 | 4.57 | Pb | 28.50 | 31.30 | 82.40 |
| Tb | 2.24 | 2.19 | 0.68 | Th | 61.80 | 93.80 | 40.00 |
| Dy | 12.20 | 12.70 | 4.04 | U | 3.18 | 5.53 | 3.43 |
| Ho | 2.22 | 2.43 | 0.81 | 10000 Ga/Al | 3.00 | 3.40 | 2.77 |

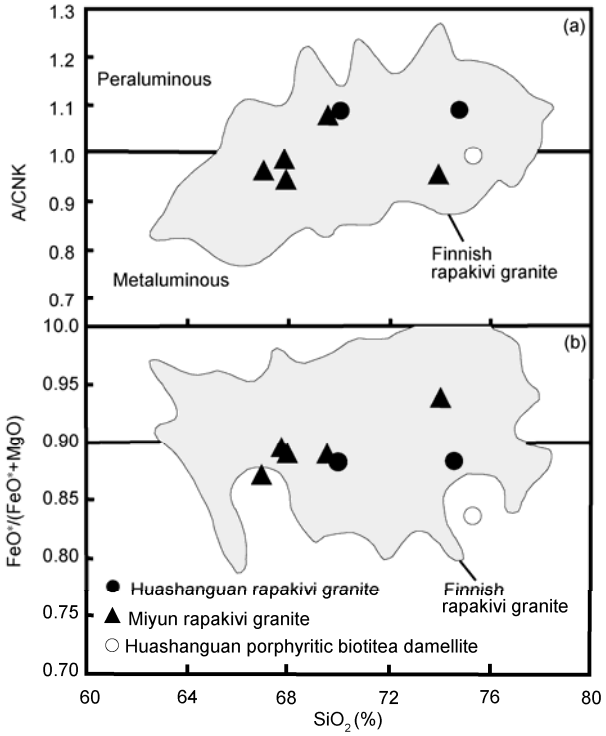


**Figure 4** The major element discrimination diagram of Huashanguan rapakivi granites. (a) A/CNK-$SiO_2$ diagram, showing that the data points cluster in the region of peraluminous rocks; (b) FeO*/(FeO*+MgO)-$SiO_2$ diagram, showing high Fe/Mg ratios. Literature comparisons for Figure 4 include the Finnish rapakivi granite [5], and data for Miyun typical rapakivi granites [7]. The diagram is adapted from [48].

to an LREE-enriched pattern. Eu showed a negative anomaly ($\delta$Eu = 0.35–0.63). However, the $\delta$Eu of the Huashanguan porphyritic biotite adamellites was only 0.07, which was strongly depleted. Huanshanguan rapakivi granites had a feature of high Th (40.0–61.8 μg $g^{-1}$), Rb (249–294 μg $g^{-1}$), Ba (915–1228 μg $g^{-1}$) and other trace elements. Conversely, the Ba content of Huashanguan porphyritic biotite adamellites was very low, only 86.2 μg$g^{-1}$. In addition, from the trace element spider diagram (Figure 5(a)), we also can see that Huashanguan rapakivi granites were similar to Finnish and Miyun typical rapakivi granites. Ba, Th, U, La, Ce, Nd and Sm were relatively enriched, and Nb, Sr, Zr and Y were relatively depleted. However, the Ba content of the Huashanguan porphyritic biotite adamellites was extremely low, indicating the chemical composition of Huashanguan porphyritic biotite adamellites differed from that of Huashanguan rapakivi granites. From the diagram of chondrite-normalized REE patterns (Figure 5(b)), we can see that the two samples of Huashanguan rapakivi granites displayed similar chondrite-normalized REE patterns with significantly-enriched light REE, fractionated heavy REE, and weakly negative Eu anomalies. These characteristics are very similar to those of Finnish and Miyun typical rapakivi granites.

### 4.2 Zircon U-Pb age and characteristics of rare earth element content

The zircons (sample ZX21-1) of the Huashanguan rapakivi granites mainly were light yellow. The shape of most zircons was semi-cylindrical columnar and fragmentation, and a minority were equant grains. Their lengths ranged from 80 and 200 μm, with aspect ratios of 1.5∶1 to 2∶1. The zircon CL images (Figure 6) show that most of the zircons had magmatic oscillatory zoning, but since Th, U contents of part of the zircons were high, the CL images were relatively dark. Zircon Th/U ratios varied from 0.78 to 1.64, which also is consistent with characteristics of magmatic zircons [51].

Twenty-one individual U-Pb spots were done on 21 zircon grains using LA-ICP-MS, and the results are shown in Tables 2 and 3. Among the 21 points, the signal of point 10 showed fluctuations, and the reverse was not harmonic. Thus, these data were not used. The unharmonious ages of the remaining 20 points gave a concordia line with upper intercept at 1901±45 Ma and lower intercept at 803±170 Ma (MSWD = 2.9) (Figure 7). The unharmonious degree and

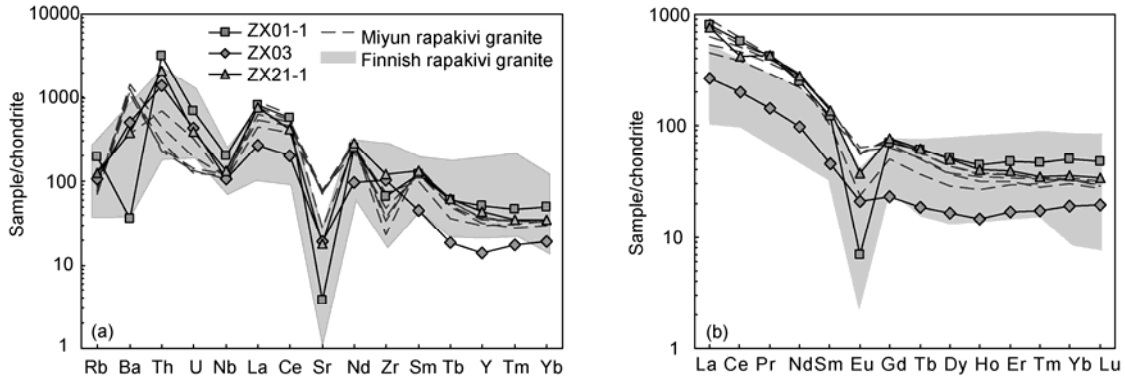


**Figure 5** Diagrams of chondrite-normalized trace element spider and chondrite-normalized REE distribution patterns of Huashanguan rapakivi granites. Literature comparisons in (a) and (b) include Finnish rapakivi granite components [49], and Miyun rapakivi granites [6]. Chondrite-normalized values are from [50].

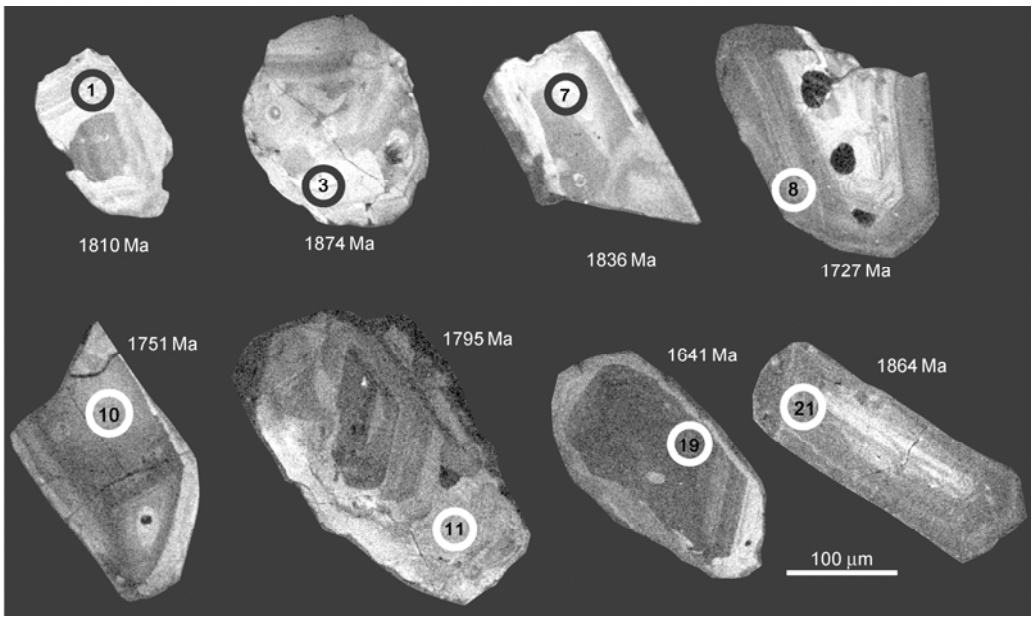


**Figure 6** Representative zircon CL images of Huashanguan rapakivi granites.

Th and U contents of points 9, 12, 18 and 19 were higher than others, and $^{207}Pb/^{206}Pb$ concordia ages were significantly lower, which indicates a possible variable proportion of grains that had lost some $^{207}Pb$ and $^{206}Pb$. Point 8 was relatively harmonic, while the age was significantly lower. From the CL image, we can see the analysis point was at the edge of the zircon, which may be due to post-recrystallization. After removing points 8, 9, 10, 12, 18 and 19, the 15 remaining higher harmonic degree analyses yielded a $^{207}Pb/^{206}Pb$ weighted mean age of 1851±18 Ma (95% confidence limits, MSWD = 1.2; Figure 7), which is consistent with the upper intercept age, representing the emplacement age of Huashanguan rapakivi granite intrusions.

CL images (Figure 6) show that the zircon oscillatory zoning of the Huashanguan rapakivi granites is vague. It is unknown if this due to the fluids. From the chondrite normalized REE distribution patterns of zircon (Figure 8), we can see that the LREE contents of zircons from Huashanguan rapakivi granites were low, and the Ce positive anomalies were obvious, which indicates an apparently magmatic origin. However, zircons of hydrothermal origin generally are characterized by high LREE content and weak Ce positive anomalies [52,53]. Thus, the zircon REE characteristics of the Huashanguan rapakivi granites were different from that of a fluid origin. The phenomenon of vague zircon oscillatory zoning may be related to metamorphic recrystallization. However, the zircon U-Pb concordia curve (Figure 7) shows that the analyses all plot on or near the concordia line, which indicates that the U-Pb systems of most zircons remained closed. These results indicate that we can obtain reliable $^{207}Pb/^{206}Pb$ ages for these samples. From the zircon U-Pb ages we can see that the lead of some zircons was lost. This may be mainly related to metamorphic recrystallization caused by later thermal events (especially the strong Neoproterozoic magmatism), and this process also can cause vagueness of the oscillatory zoning. The lower intercept age (ca. 800 Ma) may represent the time when the rock suffered a later thermal event, which also is consistent with the time of Neoproterozoic tectonothermal events in the Yangtze block, or even over the entire South China area [54–63].

## 5 Discussion

### 5.1 Rapakivi textures

The origin of rapakivi textures has been a long, contentious geological issue lasting more than 100 years. Haapala et al. [2] and Rämö et al. [3] have ever discussed this problem. In short, the origin can be divided into two categories: magmatic model and post-magmatic exsolution-component adjustment mode. Current studies have shown that a magma mixing mode and sub-isothermal decompression mode of crystal saturated granitic magma (magma mode) are possible. The magma mixing mode stresses the disequilibrium of the texture resulted by the mixing process of felsic and mafic magmas [64]. The sub-isothermal decompression mode stresses partial resortion of alkali feldspar and quartz, and continued crystallization of plagioclase around the alkali feldspar resulted by magma decompression and slow cooling [65]. This origin model has been confirmed by Eklund et al. [66]. According to petrographic observations, the origin of Huashanguan rapakivi textures also should be that of magma crystallization. For example, from the relationship between minerals, it is evident that K-feldspar phenocrysts enwrap almost all the minerals in the rocks. The small

**Table 2** Results of zircon U-Pb isotopic data obtained by LA-ICP-MS from sample ZX21-1 of Huashanguan rapakivi granite.

| Analyses | Pb (μg g$^{-1}$) total | $^{232}$Th (μg g$^{-1}$) | $^{238}$U (μg g$^{-1}$) | Ratios and error | | | | | | | | |
|---|---|---|---|---|---|---|---|---|---|---|---|---|
| | | | | $^{207}$Pb/$^{206}$Pb | 1$\sigma$ | $^{207}$Pb/$^{235}$U | 1$\sigma$ | $^{206}$Pb/$^{238}$U | 1$\sigma$ | $^{208}$Pb/$^{232}$Th | 1$\sigma$ | $^{232}$Th/$^{238}$U |
| ZX21-1-1 | 48 | 117 | 109 | 0.1153 | 0.0021 | 5.2586 | 0.0948 | 0.3260 | 0.0037 | 0.0993 | 0.0016 | 0.9955 |
| ZX21-1-2 | 32 | 78 | 76 | 0.1099 | 0.0021 | 4.9315 | 0.1081 | 0.3200 | 0.0045 | 0.0896 | 0.0015 | 0.9767 |
| ZX21-1-3 | 45 | 96 | 113 | 0.1146 | 0.0016 | 5.0553 | 0.0860 | 0.3133 | 0.0031 | 0.0866 | 0.0011 | 0.7807 |
| ZX21-1-4 | 101 | 348 | 209 | 0.1125 | 0.0013 | 5.1109 | 0.0734 | 0.3231 | 0.0033 | 0.0935 | 0.0011 | 1.5740 |
| ZX21-1-5 | 24 | 60 | 58 | 0.1135 | 0.0023 | 4.8500 | 0.1065 | 0.3041 | 0.0037 | 0.0896 | 0.0014 | 0.9699 |
| ZX21-1-6 | 14 | 37 | 33 | 0.1149 | 0.0034 | 4.9347 | 0.1378 | 0.3080 | 0.0048 | 0.0931 | 0.0034 | 1.0579 |
| ZX21-1-7 | 57 | 137 | 120 | 0.1122 | 0.0020 | 5.5081 | 0.1222 | 0.3489 | 0.0063 | 0.1080 | 0.0017 | 1.0959 |
| ZX21-1-8 | 190 | 511 | 426 | 0.1139 | 0.0020 | 5.0954 | 0.0981 | 0.3182 | 0.0054 | 0.0992 | 0.0014 | 1.1541 |
| ZX21-1-9 | 407 | 1549 | 1362 | 0.1052 | 0.0021 | 3.2469 | 0.0685 | 0.2207 | 0.0050 | 0.0721 | 0.0012 | 1.1123 |
| ZX21-1-10 | 209 | 478 | 426 | 0.1071 | 0.0024 | 5.4578 | 0.1425 | 0.3626 | 0.0085 | 0.1094 | 0.0023 | 1.0775 |
| ZX21-1-11 | 41 | 94 | 97 | 0.1097 | 0.0027 | 5.2298 | 0.1452 | 0.3370 | 0.0073 | 0.0926 | 0.0021 | 0.9321 |
| ZX21-1-12 | 303 | 1022 | 1096 | 0.1073 | 0.0021 | 3.2228 | 0.0715 | 0.2136 | 0.0041 | 0.0698 | 0.0013 | 0.9391 |
| ZX21-1-13 | 46 | 123 | 105 | 0.1130 | 0.0024 | 5.4106 | 0.1197 | 0.3402 | 0.0061 | 0.0946 | 0.0018 | 1.1347 |
| ZX21-1-14 | 407 | 1363 | 994 | 0.1114 | 0.0021 | 4.3713 | 0.1029 | 0.2793 | 0.0052 | 0.0947 | 0.0018 | 1.3444 |
| ZX21-1-15 | 165 | 337 | 386 | 0.1153 | 0.0025 | 5.6289 | 0.1395 | 0.3485 | 0.0065 | 0.1022 | 0.0023 | 0.8279 |
| ZX21-1-16 | 185 | 362 | 431 | 0.1169 | 0.0025 | 5.8087 | 0.1598 | 0.3559 | 0.0081 | 0.1032 | 0.0023 | 0.8074 |
| ZX21-1-17 | 64 | 215 | 144 | 0.1158 | 0.0026 | 5.1443 | 0.1520 | 0.3174 | 0.0072 | 0.0953 | 0.0019 | 1.4489 |
| ZX21-1-18 | 397 | 1707 | 1687 | 0.0995 | 0.0019 | 2.4924 | 0.0571 | 0.1783 | 0.0030 | 0.0623 | 0.0012 | 0.9875 |
| ZX21-1-19 | 255 | 1436 | 851 | 0.1150 | 0.0023 | 3.1790 | 0.0715 | 0.1991 | 0.0039 | 0.0620 | 0.0013 | 1.6388 |
| ZX21-1-20 | 675 | 2086 | 1537 | 0.1251 | 0.0022 | 5.3561 | 0.1111 | 0.3061 | 0.0043 | 0.0959 | 0.0017 | 1.3173 |
| ZX21-1-21 | 211 | 626 | 500 | 0.1140 | 0.0023 | 4.8861 | 0.1079 | 0.3088 | 0.0052 | 0.0930 | 0.0017 | 0.8319 |

| Analyses | Discordant age (Ma) | | | | | | | | Concordant age (Ma) | | | | | | | |
|---|---|---|---|---|---|---|---|---|---|---|---|---|---|---|---|---|
| | $^{207}$Pb/$^{206}$Pb | 1$\sigma$ | $^{207}$Pb/$^{235}$U | 1$\sigma$ | $^{206}$Pb/$^{238}$U | 1$\sigma$ | $^{208}$Pb/$^{232}$Th | 1$\sigma$ | $^{207}$Pb/$^{206}$Pb | 1$\sigma$ | $^{207}$Pb/$^{235}$U | 1$\sigma$ | $^{206}$Pb/$^{238}$U | 1$\sigma$ | $^{208}$Pb/$^{232}$Th | 1$\sigma$ |
| ZX21-1-1 | 1885 | 26 | 1862 | 15 | 1819 | 18 | 1914 | 30 | 1810 | 62 | 1807 | 26 | 1805 | 20 | 1804 | 20 |
| ZX21-1-2 | 1798 | 31 | 1808 | 18 | 1790 | 22 | 1734 | 28 | 1798 | 31 | 1808 | 18 | 1790 | 22 | 1734 | 28 |
| ZX21-1-3 | 1874 | 25 | 1829 | 14 | 1757 | 15 | 1678 | 20 | 1874 | 25 | 1829 | 14 | 1757 | 15 | 1678 | 20 |
| ZX21-1-4 | 1839 | 19 | 1838 | 12 | 1805 | 16 | 1807 | 21 | 1839 | 19 | 1838 | 12 | 1805 | 16 | 1807 | 21 |
| ZX21-1-5 | 1856 | 34 | 1794 | 18 | 1712 | 18 | 1735 | 27 | 1856 | 34 | 1794 | 18 | 1712 | 18 | 1735 | 27 |
| ZX21-1-6 | 1878 | 43 | 1808 | 24 | 1731 | 23 | 1800 | 63 | 1878 | 43 | 1808 | 24 | 1731 | 23 | 1800 | 63 |
| ZX21-1-7 | 1836 | 24 | 1902 | 19 | 1930 | 30 | 2073 | 30 | 1836 | 24 | 1902 | 19 | 1930 | 30 | 2073 | 30 |
| ZX21-1-8 | 1862 | 17 | 1835 | 16 | 1781 | 26 | 1911 | 26 | 1727 | 90 | 1744 | 36 | 1759 | 30 | 1762 | 29 |
| ZX21-1-9 | 1719 | 19 | 1468 | 16 | 1285 | 26 | 1407 | 23 | 1456 | 127 | 1336 | 44 | 1262 | 30 | 1248 | 28 |
| ZX21-1-10 | 1751 | 22 | 1894 | 22 | 1995 | 40 | 2099 | 41 | 1751 | 22 | 1894 | 22 | 1995 | 40 | 2099 | 41 |
| ZX21-1-11 | 1795 | 32 | 1857 | 24 | 1872 | 35 | 1791 | 39 | 1795 | 32 | 1857 | 24 | 1872 | 35 | 1791 | 39 |
| ZX21-1-12 | 1754 | 22 | 1463 | 17 | 1248 | 22 | 1364 | 25 | 1555 | 102 | 1352 | 36 | 1228 | 24 | 1207 | 22 |
| ZX21-1-13 | 1848 | 24 | 1887 | 19 | 1887 | 29 | 1826 | 34 | 1848 | 24 | 1887 | 19 | 1887 | 29 | 1826 | 34 |
| ZX21-1-14 | 1822 | 27 | 1707 | 19 | 1588 | 26 | 1828 | 33 | 1822 | 27 | 1707 | 19 | 1588 | 26 | 1828 | 33 |
| ZX21-1-15 | 1884 | 30 | 1921 | 21 | 1927 | 31 | 1967 | 42 | 1884 | 30 | 1921 | 21 | 1927 | 31 | 1967 | 42 |
| ZX21-1-16 | 1909 | 28 | 1948 | 24 | 1963 | 39 | 1985 | 43 | 1909 | 28 | 1948 | 24 | 1963 | 39 | 1985 | 43 |
| ZX21-1-17 | 1893 | 35 | 1843 | 25 | 1777 | 35 | 1840 | 35 | 1893 | 35 | 1843 | 25 | 1777 | 35 | 1840 | 35 |
| ZX21-1-18 | 1616 | 30 | 1270 | 17 | 1058 | 16 | 1221 | 23 | 1202 | 117 | 1087 | 37 | 1030 | 18 | 1021 | 17 |
| ZX21-1-19 | 1881 | 20 | 1452 | 17 | 1170 | 21 | 1216 | 24 | 1641 | 145 | 1332 | 53 | 1149 | 26 | 1119 | 22 |
| ZX21-1-20 | 2031 | 27 | 1878 | 18 | 1721 | 21 | 1851 | 31 | 1846 | 88 | 1762 | 37 | 1692 | 25 | 1678 | 24 |
| ZX21-1-21 | 1864 | 26 | 1800 | 19 | 1735 | 26 | 1797 | 32 | 1864 | 26 | 1800 | 19 | 1735 | 26 | 1797 | 32 |

**Table 3** Results of zircon rare earth element (REE) values (μg $g^{-1}$) from sample ZX21-1 of Huashanguan rapakivi granite

| Analyses | La | Ce | Pr | Nd | Sm | Eu | Gd | Tb | Dy | Ho | Er | Tm | Yb | Lu |
|---|---|---|---|---|---|---|---|---|---|---|---|---|---|---|
| ZX21-1-1 | 0.10 | 18.27 | 0.13 | 1.68 | 2.99 | 0.14 | 13.72 | 4.39 | 51.15 | 18.56 | 90.85 | 20.3 | 196.08 | 36.20 |
| ZX21-1-2 | 0.04 | 14.66 | 0.06 | 0.77 | 2.07 | 0.12 | 8.79 | 3.2 | 38.87 | 13.9 | 68.99 | 14.99 | 138.47 | 25.34 |
| ZX21-1-3 | 0.01 | 14.15 | 0.04 | 1.18 | 2.23 | 0.08 | 10.57 | 3.52 | 43.08 | 15.25 | 78.32 | 17.1 | 162.6 | 28.29 |
| ZX21-1-4 | 0.22 | 24.37 | 1.46 | 18.42 | 19.76 | 0.82 | 73.87 | 20.43 | 229.26 | 76.54 | 345.76 | 65.74 | 579.56 | 97.57 |
| ZX21-1-5 | 0.02 | 12.8 | 0.06 | 1.24 | 1.83 | 0.13 | 10.25 | 2.99 | 37.34 | 13.72 | 66.18 | 14.33 | 138.95 | 23.34 |
| ZX21-1-6 | 0.01 | 10.82 | 0.08 | 1.33 | 1.83 | 0.17 | 9.16 | 2.8 | 35.08 | 12.13 | 61.11 | 13.35 | 131.29 | 24.15 |
| ZX21-1-7 | 0.14 | 18.4 | 0.25 | 4.07 | 6.19 | 0.27 | 23.38 | 7.35 | 83.35 | 28.52 | 137.02 | 28.34 | 259.46 | 44.21 |
| ZX21-1-8 | 0.12 | 21.79 | 0.45 | 7.28 | 9.48 | 0.29 | 48.49 | 15.42 | 184.28 | 65.75 | 314.68 | 68.63 | 652.98 | 109.16 |
| ZX21-1-9 | 0.14 | 42.04 | 0.79 | 9.09 | 15.18 | 0.37 | 68.85 | 23.35 | 297.38 | 110.41 | 542.13 | 119.3 | 1111.18 | 174.92 |
| ZX21-1-10 | 0.25 | 24.58 | 0.58 | 8.66 | 13.4 | 0.26 | 58.99 | 18.49 | 219.62 | 75.1 | 344.31 | 71.43 | 656.49 | 104.78 |
| ZX21-1-11 | 0.01 | 16.97 | 0.07 | 1.02 | 1.94 | 0.09 | 9.87 | 3.4 | 41.02 | 15.17 | 75.99 | 16.57 | 160.91 | 27.81 |
| ZX21-1-12 | 0.06 | 29.84 | 0.6 | 11.04 | 15.08 | 0.47 | 59.07 | 20.87 | 259.79 | 95.49 | 469.03 | 103.9 | 997.69 | 152.85 |
| ZX21-1-13 | 0 | 20.11 | 0.11 | 1.41 | 3.33 | 0.17 | 16.01 | 4.88 | 59.49 | 20.26 | 99.43 | 21.24 | 201.15 | 33.12 |
| ZX21-1-14 | 0.1 | 37.93 | 0.82 | 11.65 | 19.54 | 0.47 | 82.4 | 25.95 | 307.78 | 109.35 | 513.86 | 112.61 | 1035.74 | 156.4 |
| ZX21-1-15 | 0.01 | 20.98 | 0.15 | 2.34 | 5.23 | 0.1 | 26.5 | 8.93 | 105.83 | 38.68 | 185.71 | 41.08 | 393.83 | 61.47 |
| ZX21-1-16 | 0.16 | 25.71 | 1.14 | 16.13 | 18.05 | 0.83 | 64.56 | 18.76 | 205.02 | 67.68 | 311.02 | 63.38 | 570.73 | 87.56 |
| ZX21-1-17 | 0.08 | 22.41 | 0.64 | 10.11 | 14.79 | 0.7 | 56.61 | 15.14 | 166.7 | 54.23 | 240.5 | 49.48 | 475.23 | 75.32 |
| ZX21-1-18 | 0.92 | 37.32 | 0.94 | 12.79 | 16.41 | 0.56 | 79.93 | 27.89 | 366.61 | 133.99 | 664.96 | 150.28 | 1401.19 | 215.1 |
| ZX21-1-19 | 0.92 | 52.16 | 1.02 | 10.78 | 13.72 | 0.36 | 50.34 | 15.92 | 190.99 | 66.21 | 324.01 | 70.1 | 681.78 | 110.6 |
| ZX21-1-20 | 0.75 | 45.52 | 1.42 | 18.85 | 24.08 | 0.53 | 113.56 | 36.25 | 450.87 | 159.76 | 758.62 | 161.83 | 1507.12 | 224.2 |
| ZX21-1-21 | 0.18 | 29.41 | 0.47 | 6.81 | 11.02 | 0.37 | 47.59 | 13.91 | 172.47 | 60.22 | 292.87 | 63.08 | 610.78 | 92.31 |

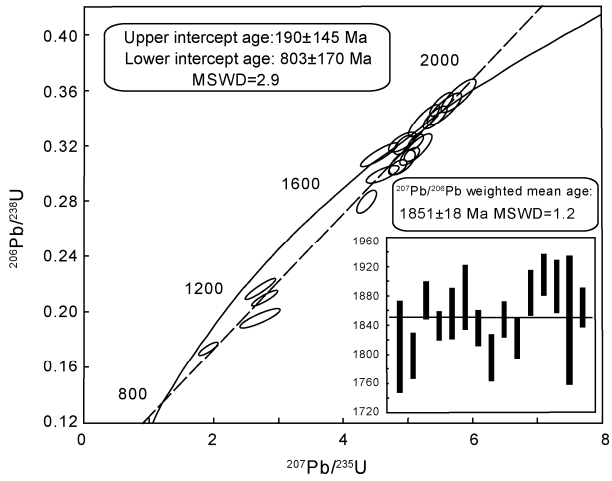


**Figure 7** Zircon U-Pb concordia curve of Huashanguan rapakivi granites.

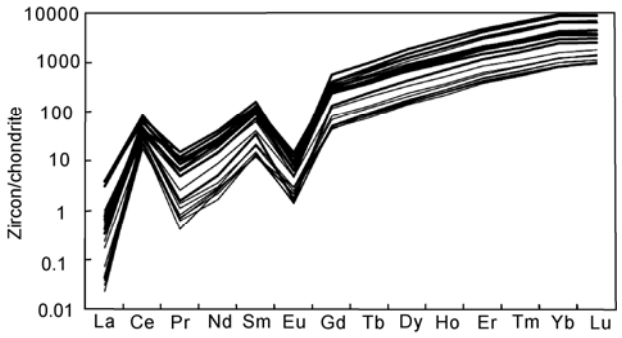


**Figure 8** Zircon chondrite-normalized REE distribution patterns of Huashanguan rapakivi granites (chondrite-normalized values from [50]).

wrapped minerals show a spherical distribution, which is parallel to the surface of the megacrysts. This indicates that during the growth process of K-Feldspar phenocrysts, the slowly growing minerals congregate at the top of the K-feldspar phenocrysts while they are rotating. Only the convection of magma can meet this condition [67]. This means that rapakivi feldspars of Huashanguan are products of magmatic crystallization.

Haapala et al. [1] defined rapakivi granites as A-type granites characterized by the presence, at least in the larger batholiths, of granite varieties showing the rapakivi textures. S-type or I-type granites with this texture are not within the range of rapakivi granites [2,3]. In fact, rapakivi granites from Late Archaean to Tetiary, including intermediate-felsic to felsic rocks. However, according currently available information, the overwhelming majority of occurrences represent granitic rocks of Proterozoic AMCG assemblages (anorthosite, monzonite, charnockite and rapakivi granites). AMCG assemblages are formed in extensional tectonic settings. It is emphasized that they are related to mantle upwelling, melting and decompression of the upper mantle, and magmatic underplating after cratonization of continental crust [3,7].

Petrographic and geochemical studies indicate that Huashanguan rapakivi granites not only have the typical rapakivi textures, but also can be correlated with A-type granites in their chemical composition, which is consistent with the definition of rapakivi granites [1]. Figure 9 shows

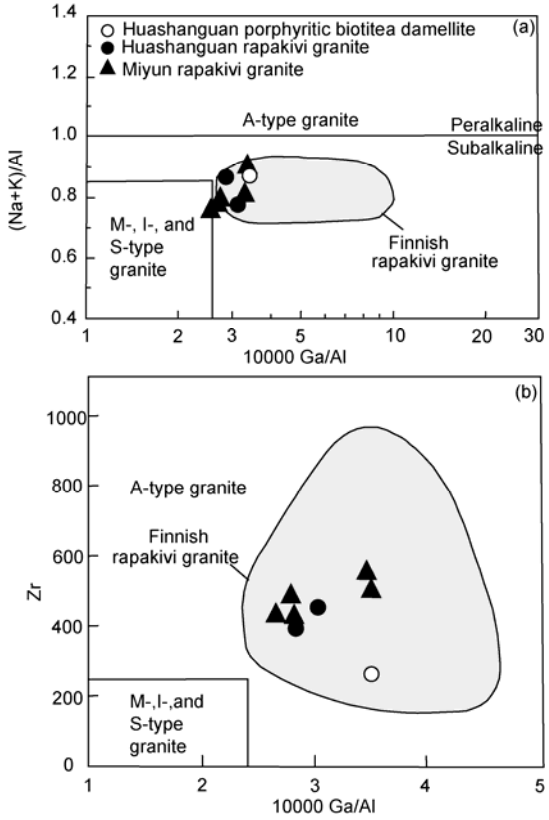


**Figure 9** Major and trace element discriminant diagrams of Huashanguan rapakivi granites. (a) (Na+K)/Al-10000 Ga/Al diagram. Data points of the Huashanguan rapakivi granites plot in the subalkaline A-type granite area; (b) Zr-10000 Ga/Al diagram. The points fall within A-type granite areas. Finnish rapakivi granite components of Figure 8(a) and (b) are from [49, 68]. Miyun typical rapakivi granite data are from [7]. The diagrams are from [48].

that Huashanguan rapakivi granites belong to A-type granites of sub-alkaline series. They fall within the Finnish typical rapakivi granite composition field, and are similar to the Miyun rapakivi granites. The major elements of Huashanguan rapakivi granites are rich in silicon, alkalis (especially rich in K) and iron, with high FeO*/MgO ratios, and low calcium and magnesium content. The rocks are rich in Th, U, La, Ga, Ce and Sm, and poor in Sr, Nb and Y, and characterized by LREE enrichment, HREE depletion and a negative Eu anomaly, which also are consistent with the affinity of rapakivi granites. Although we have not found the equivalent of AMCG assemblages in this district yet, there is evidence of contemporary mafic magmatic activity near the Huashanguan rapakivi granites. For example, Peng et al. [37] found contemporary (~1.85 Ga) mafic dikes in the Kongling high-grade metamorphic terrain, not far from the Huashanguan rapakivi pluton in the Yangtze block. This finding indicates the existence of bimodal magmatic associations.

However, Rämö et al. [3] noted that "each rapakivi pluton has its own peculiarities." It is important to understand how these granites differ from the typical rapakivi granites of Finland, Miyun and other places, and why it appears that the Huashanguan rapakivi granitic intrusions are smaller and with few appearance of amphibole. Instead, these granites contain mainly biotite, reflecting a higher water fugacity in the magma chamber than that of other rapakivi granitic plutons. This may be the reason why rapakivi granites in this area have a limited distribution. In addition, Rb/Sr and Rb/Ba ratios of Huashanguan rapakivi granites were relatively higher, which means that the intrusions had experienced a high degree of magma crystallization differentiation.

### 5.2 Tectonic significance of Paleoproterozoic rapakivi granites in the Yangtze block

A series of global super-events took place during the Paleoproterozoic. These events may match the global collisional orogenic and amalgamation events in relation to the formation of the Columbia supercontinent [13,69,70], the rapid growth of continental crust [71,72], and activities of super-mantle plumes [73]. Studies on Paleoproterozoic tectonic magmatic events are relatively few in the Yangtze block, but in recent years, more Paleoproterozoic records of geological events have been described and discussions about the evolution of the geological events, global tectonic setting and their significance have been taken place.

The existence of the Paleoproterozoic Columbia supercontinent has been widely recognized. There are many records of Paleoproterozoic large-scale tectonothermal events associated with amalgamation and breakup of the Columbia supercontinent in the North China block [10,15,24]. The latest research shows that there are many chronological records of the widespread 2.1–1.8 Ga tectonothermal events in the Yangtze block.

(1) 2.1–2.0 Ga magmatic events. Magmatic bodies of this period have not been found in the Yangtze block so far. However, detrital zircon geochronology shows that the Yangtze block has produced a wide range of 2.1–2.0 Ga zircons in the Neoproterozoic sedimentary rocks. They show oscillatory zoning and have high Th/U ratios (~1.0). It is clear that they are of magmatic origins [74,75]. In addition, researchers have obtained ca. 2000 Ma zircon xenocryst ages (using LA-ICPMS, the majority of zircons have Th/U>1) in the lamproite around the Yangtze block [30]. Furthermore, 2091–2025 Ma old zircon ages were measured in Mesozoic zircons of the Tongling district, Anhui Province (SHRIMP method, Th/U is 0.15–0.46, with oscillatory zoning) [76]. These all indicate 2.1–2.0 Ga magmatic events are widely represented in the Yangtze block.

(2) 2.0–1.9 Ga metamorphic events. Examples of events of this age range can be found in the Huangtuling granulite of the Dabie Mountains (1992 Ma, zircon evaporation [77]; 1998±35 Ma, garnet dissolving gradually [78]; 2052±100 Ma, LA-ICPMS [79]; 2002±17 Ma, SIMS [80]); gneiss and

amphibolites of the Kongling Group in the Kongling metamorphic terrain (1939±44 and 1958±15 Ma, Sm-Nd isochron) [81]; trondhjemite and metamorphic pelitic rocks (1990±16 Ma and 1930±50 Ma, SHRIMP [27]; 1992±16 Ma and 1928±18 Ma, SHRIMP [82]; metamorphic pelitic rocks and amphibolites (1950±50 Ma, 1980±20 Ma and 1940±40 Ma, LA-ICPMS) [34] and mixed rocks (1980–2013 Ma, SHRIMP) [83]. These chronological records are distributed across the northern margin of the Yangtze block, and may represent a collisional orogenic events [34] related to the amalgamation of the Columbia supercontinent [29,34,35].

(3) ~1.85 Ga extensional rifting events. Rapakivi granites were formed in an anorogenic or post-orogenic tectonic environment, and are considered to be one of the extensional environmental indicators [1]. The Huashanguan granites reported in this paper belong to the typical rapakivi granites. Dating results show that the pluton was formed at about 1850 Ma in the late Paleoproterozoic. Conversely, the orogenic events related to the amalgamation of the Columbia supercontinent took place at 2.0–1.9 Ga, just before the formation time of Huashanguan rapakivi granite intrusions. In addition, the formation time of mafic dikes, marking regional extension found in the Kongling high-grade metamorphic terrain, also were about 1.85 Ga [37]. Besides, the formation age of the Quanyishang A-type granites recently reported is about 1.85 Ga. Zircon Hf isotopic studies show that the source of Quanyishang A-type granites may come from the Archean crust deep in the Yangtze continent, and that this source may be related to the extension and collapse of the deep crust with Archean ages, in response to the transition stage of the assembly and breakup of the Columbia supercontinent [36]. While the source of the Huashanguan rapakivi granites reported in this paper is unknown, it is possible that it may be from the deep Archean continental crust. Further isotope studies may confirm this assertion. However, the Huashanguan rapakivi granites, Quanyishang A-type granites and mafic dikes in the Kongling high-grade metamorphic terrain were all formed in the extensional tectonic setting, which indicates that they occurred in the tectonic transformation from collision to extension at about 1.85 Ga in the Yangtze block, and may be associated with breakup of the Columbia supercontinent.

In summary, there are many chronological records of the widespread 2.1–1.8 Ga tectonothemal events in the Yangtze block. These may represent the evolutionary history of supercontinent amalgamation to breakup. In other words, they may belong to part of the amalgamation and breakup process of the Paleoproterozoic Columbia supercontinent. The discovery of 1.85 Ga Huashanguan rapakivi granites provides important evidence for the formation and cratonization of the Yangtze block in the Paleoproterozoic, and for its later tectonic transformation from collision to extension. Recently, there have been reports on orogenic events of 1.89–1.83 Ga [84], and breakup events of 1.80–1.76 Ga [85–87] in the Cathaysian block. These events took place a little later than those in the Yangtze block, which indicates that the two blocks may have been located in different positions in the supercontinent system. Therefore, they had different evolution histories.

## 6 Conclusions

(1) Huashanguan rapakivi granites have typical rapakivi textures. They are characterized by the ovoidal shapes of their alkali feldspar megacryst, being mantled with oligoclase-andesine shells, and both the alkali feldspar and quartz generally show two or more generations. Minerals wrapped in K-feldspar phenocrysts mostly show a spherical distribution. Huashanguan rapakivi granites belong to A-type granites of sub-alkaline, peraluminous, high Fe/Mg ratios and with typical rapakivi texture.

(2) Zircon U-Pb dating shows that the emplacement age of the Huashanguan rapakivi granite pluton was 1851±18 Ma. The lower intercept U-Pb age of 803±170 Ma may represent the time that the intrusion was affected by the later Neoproterozoic tectonic events.

(3) The research shows that there may have been widespread late Paleoproterozoic (ca. 2000 Ma) magmatic and metamorphic events associated with the amalgamation and breakup of supercontinent masses in the Yangtze block. The later development of 1.85 Ga Huashanguan rapakivi granites indicates that the Yangtze block was in a continental breakup or post-orogenic extensional tectonic setting at 1.85 Ga, which may be related to the breakup of the Paleoproterozoic Columbia supercontinent.

*We would like to acknowledge the assistance and guidance from Profs. Ling Wenli, Paul Robinson and Eric H. Christiansen through the writing and revisions, and the constructive comments and suggestions provided by two peer reviewers, editors and editorial board. This work was supported by the International Cooperation Project of the Ministry of Science and Technology of China (2007DFA21230), the Natural Science Foundation of Hubei Province (2009CDA004), the National Training Foundation of Geological Science Base (J083520) and the National Innovation Experiment Program for University Students (1320311009). This study was part of a Higher Education Key Project of Hubei Province (2009108).*

1 Haapala I, Rämö O T. Tectonic setting and origin of the Proterozoic rapakivi granites of the southeastern Fennoscandia. Trans Roy Soc Edinburgh Earth Sci, 1992, 83: 165–171
2 Haapala I, Rämö O T. Rapakivi granites and related rocks: An introduction. Precambrian Res, 1999, 95: 1–7
3 Rämö O T, Haapala I. One hundred years of rapakivi granite. Miner Petrol, 1995, 52: 129–185
4 Väino P, Flodén T. Rapakivi-granite-anorthosite magmatism—A way of thinning and stabilization of the Svecofennian crust, Baltic Sea Basin. Tectonophysics, 1999, 305: 75–92
5 Rämö O T, Haapala I, Vaasjoki M, et al. 1700 Ma Shachang complex, northeast China: Proterozoic rapakivi granite not associated with Paleoprozoic orogenic crust. Geology, 1995, 23: 815–818
6 Xie G H. Petrology and geochemistry of the anorthosite in Damiao and the rapakivi granite in Miyun: A Review on the Global Distribution and Significance of Massif-Anorthosite and Rapakivi Granite (in Chinese). Beijing: Science Press, 2005. 1–195

7 Yu J H, Fu H X, Zhang F L, et al. Anorogenic Rapakivi Granite and Related Rocksin Northern Part of the North China Craton (in Chinese). Beijing: China Science and Technology Press, 1996. 1–182
8 Vigneresse J L. The specific case of the Mid-Proterozoic rapakivi granites and associated suite within the context of the Columbia supercontinent. Precambrian Res, 2005, 137: 1–34
9 Dall'Agnol R, Teixeira N P, Rämö O T, et al. Petrogenesis of the Paleoproterozoic rapakivi A-type granites of the Archean Carajás metallogenic province, Brazil. Lithos, 2005, 80: 101–129
10 Yang J H, Wu F Y, Liu X M, et al. Zircon U-Pb ages and Hf isotopes and their geological significance of the Miyun rapakivi granites from Beijing (in Chinese). Acta Petrol Sin, 2005, 21: 1633–1644
11 Zhao G C, Sun M, Wilde S A. Reconstruction of a Pre-Rodinia Supercontinent: New advances and perspective. Chinese Sci Bull, 2002, 47: 1585–1588
12 Zhao G C, Cawood P A, Wilde S A, et al. Review of global 2.1–1.8 Ga orogens: Implications for a pre-Rodinia supercontinent. Earth Sci Rev, 2002, 59: 125–162
13 Rogers J J W, Santosh M. Cofiguration of Columbia, a Mesoproterozoic supercontinent. Gondwana Res, 2002, 5: 5–22
14 Wang Y J, Fan W M, Zhang Y H. Geochemical, $^{40}Ar/^{39}Ar$ geochronological and Sr-Nd isotopic constraints on the origin of Paleoproterozoic mafic dikes from the southern Taihang Mountains and implications for the ca.1800 Ma event of the North China Craton. Precambrian Res, 2004, 135: 55–77
15 Wang Y J, Zhao G C, Fan W M, et al. LA-ICP-MS U-Pb zircon geochronology and geochemistry of Paleoproterozoic mafic dikes from western Shandong Province: Implications for back-arc basin magmatism in the Eastern Block, North China Craton. Precambrian Res, 2007, 154: 107–124
16 Zhai M G, Liu W J. Palaeoproterozoic tectonic history of the North China craton: A review. Precambrian Res, 2003, 122: 183–199
17 Guo J H, Sun M, Chen F K, et al. Sm-Nd and SHRIMP U-Pb zircon geochronology of high-pressure granulites in the Sanggan area, North China Craton: Timing of Paleoproterozoic continental collision. J Asian Earth Sci, 2005, 24: 629–642
18 Wan Y S, Song B, Liu D Y, et al. SHRIMP U-Pb zircon geochronology of Palaeoproterozoic metasedimentary rocks in the North China Craton: Evidence for a major Late Palaeoproterozoic tectonothermal event. Precambrian Res, 2006, 149: 249–271
19 Peng P, Zhai M G, Ernst R E, et al. A 1.78 Ga large igneous province in the North China craton: The Xiong'er Vol-canic Province and the North China dyke swarm. Lithos, 2008, 101: 260–280
20 Zhao G C, Sun M, Wilde S A, et al. Late Archean to Paleoproterozoic evolution of the North China Craton: Key issues revisited. Precambrian Res, 2005, 136: 177–202
21 Hou G T, Santosh M, Qian X L, et al. Tectonic constraints on 1.3~1.2 Ga final breakup of Columbia supercontinent from a giant radiating dyke swarm. Gondwana Res, 2008, 14: 516–566
22 Hou G T, Santosh M, Qian X L, et al. Configuration of the Late Paleoproterozoic supercontinent Columbia: Insights from radiating mafic dyke swarms. Gondwana Res, 2008, 14: 395–409
23 Kusky T, Li J H, Santosh M. The Paleoproterozoic North Hebei Orogen: North China craton's collisional suture with the Columbia supercontinent. Gondwana Res, 2007, 12: 4–28
24 Zhang S H, Liu S W, Zhao Y, et al. The 1.75–1.68 Ga anorthosite-mangerite-alkali granitoid-rapakivi granite suite from the northern North China Craton: Magmatism related to a Paleoproterozoic orogen. Precambrian Res, 2007, 155: 287–312
25 Ling W L, Gao S, Zheng H F, et al. An Sm-Nd isotopic dating of the Archean Kongling Complex in the Huangling area of the Yangtze Craton. Chinese Sci Bull, 1998, 43: 1187–1191
26 Gao S, Ling W L, Qiu Y M, et al. Contrasting geochemical and Sm-Nd isotopic compositions of Archean metasediments from the Kongling high-grade terrain of the Yangtze craton: Evidence for cratonic evolution and redistribution of REE during crustal anatexis. Geochim Cosmochim Acta, 1999, 63: 2071–2088
27 Qiu Y M, Gao S, McNaughton N J, et al. First evidence of >3.2 Ga continental crust in the Yangtze craton of south China and its implications for Archean crustal evolution and Phanerozoic tectonics. Geology, 2000, 28: 11–14
28 Zhang S B, Zheng Y F, Zhao Z F, et al. Origin of TTG-like rocks from anatexis of ancient lower crust: Geochemical evidence from Neoproterozoic granitoids in South China. Lithos, 2009, 113: 347–368
29 Wu Y B, Zheng Y F, Gao S, et al. Zircon U-Pb age and trace element evidence for Paleoproterozoic granulite facies metamorphism and Archean crustal rocks in the Dabie Orogen. Lithos, 2008, 101: 308–322
30 Zheng J P, Griffin W L, O'Reilly S Y, et al. Widespread Archean basement beneath the Yangtze craton. Geology, 2006, 34: 417–420
31 Shen Q H, Geng Y S, Song B, et al. New information from the surface outcrops and deep crust of Archean rocks of the North China and Yangtze Blocks, and Qinling-Dabie Orogenic Belt (in Chinese). Acta Geol Sin, 2005, 79: 616–627
32 Zheng Y F. Neoproterozoic magmatic activity and global change. Chinese Sci Bull, 2003, 48: 1639–1656
33 Ling W L, Gao S, Zhang B R, et al. The recognizing of ca. 1.95 Ga tectonothermal event in Kong-ling nucleus and its significance for the evolution of Yangtze Block, South China. Chinese Sci Bull, 2001, 46: 326–329
34 Zhang S B, Zheng Y F, Wu Y B, et al. Zircon U-Pb age and Hf-O isotope evidence for Paleoproterozoic metamorphic event in South China. Precambrian Res, 2006, 151: 265–288
35 Wu Y B, Gao S, Gong H J, et al. Zircon U-Pb age, trace element and Hf isotope composition of Kongling terrane in the Yangtze Craton: Refining the timing of Palaeoproterozoic high-grade metamorphism. J Metamorphic Geol, 2009, 27: 461–477
36 Xiong Q, Zheng J P, Yu C M, et al. Zircon U-Pb age and Hf isotope of Quanyishang A-type granite in Yichang: Significaation for the Yangtze continental cratonization in Paleoproterozoic. Chinese Sci Bull, 2008, 54: 436–446
37 Peng M, Wu Y B, Wang J, et al. Paleoproterozoic mafic dikes from Kongling terrain in the Yangzte Craton and its implication. Chinese Sci Bull, 2009, 54: 1098–1104
38 Zhao G C, Sun M, Wilde S A, et al. A Paleo-Mesoproterozoic supercontinent: Assembly, growth and breakup. Earth Sci Rev, 2004, 67: 91–123
39 Hubei Provincial Bureau of Geological and Mineral Resource. Regional Geology of Hubei Province. Beijing: Geological Publishing House, 1990. 1–662
40 Sederholm J J. Ueber die finnlandischen Rapakiwigesteine. Tschermaks Miner Petrogr Mitt, 1891, 12: 1–31
41 Hu N G, Wang X X, Sun Y G, et al. The geochemistry features, origin of the Yingfeng rapakivi granite and its associated rocks in north Qaidam basin and the geological significance (in Chinese). Geol Rev, 2007, 53: 460–472
42 Xiao Q H, Lu X X, Wang F, et al. Age of Yingfeng rapakivi granite pluton on the north flank of Qaidam and its geological significance. Sci China Ser D-Earth Sci, 2004, 47: 357–365
43 Gao S, Zhang B R, Gu X M, et al. Silurian-Devonian provenance changes of South Qinling basins: Implications for accretion of the Yangtze (South China) to the North China cratons. Tectonophysics, 1995, 250: 183–197
44 Zhang H F, Gao S, Zhong Z Q, et al. Geochemical and Sr-Nd-Pb isotopic compositions of Cretaceous granitoids: Constraints on tectonic framework and crustal structure of the Dabieshan ultrahigh-pressure metamorphic belt, China. Chem Geol, 2002, 186: 281–299
45 Liu Y S, Gao S, Hu Z C, et al. Continental and Oceanic Crust Recycling-induced Melt-Peridotite Interactions in the Trans-North China Orogen: U-Pb Dating, Hf Isotopes and Trace Elements in Zircons from Mantle Xenoliths. J Petrol, 2010, 51: 537–571
46 Andersen T. Correction of common lead in U-Pb analyses that do not report $^{204}Pb$. Chem Geol, 2002, 192: 59–79
47 Ludwig K R. Users manual for Isoplot 3.00: A geochronological toolkit for Microsoft Exccel. Berkeley Geochron Cent Spec Publ, 2003, 4: 1–70
48 Whalen J B, Currie K L, Chappell B W. A-type granites: Geochemi-

cal characteristics, discrimination and petrogenesis. Contrib Miner Petrol, 1987, 95: 407–419
49 Haapala I, Rämö O T, Frindt S. Comparison of Proterozoic and Phanerozoic rift-related basaltic-granitic magmatism. Lithos, 2005, 80: 1–32
50 McDonough W F, Sun S S. The composition of the Earth. Chem Geol, 1995, 120: 223–253
51 Wu Y B, Zheng Y F. Genesis of zircon and its constraints on interpretation of U-Pb ages. Chinese Sci Bull, 2004, 49: 1554–1569
52 Hoskin P W O. Trace-element composition of hydrothermal zircon and the alteration of Hadean zircon from the Jack Hills, Australia. Geochim Cosmochim Acta, 2005, 69: 637–648
53 Pelleter E, Cheilletz A, Gasquet D, et al. Hydrothermal zircons: A tool for ion microprobe U-Pb dating of gold mineralization (Tamlalt-Menhouhou gold deposit-Morocco). Chem Geol, 2007, 245: 135–161
54 Ling W L, Wang X H, Cheng J P. Geochemical features and tectonic implication of the Jinningian Wangjiangshan gabbros in the north margin of Yangtze block (in Chinese). Bull Miner Petrol Geochem, 2001, 20: 218–221
55 Zeng W, Zhong Z Q, Zhou H W, et al. Geochemistry of mafic dykes in Huangling area and its tectonic implications (in Chinese). Earth Sci-J Chin Univ Geosci, 2004, 29: 31–38
56 Ling W L, Gao S, Cheng J P, et al. Neoproterozoic magmatic events within the Yangtze continental interior and along its northern margin and their tectonic implication: Constraint from the ELA-ICPMS U-Pb geochronology of zircon from the Huangling and Hannan complexes (in Chinese). Acta Petrol Sin, 2006, 22: 387–396
57 Ling W L, Gao S, Zhang B R, et al. Neoproterozoic tectonic evolution of the northwestern Yangtze craton, South China: Implications for amalgamation and break-up of the Rodinia Supercontinent. Precambrian Res, 2003, 122: 111–140
58 Li X H, Li W X, Qiu L L, et al. Petrogenesis and tectonic significance of the ~850 Ma Gangbian alkaline complex in South China: Evidence from in situ zircon U-Pb dating, Hf-O isotopes and whole-rock geochemistry. Lithos, 2010, 114: 1–15
59 Wang X L, Zhou J C, Qiu J S, et al. LA-ICP-MS U-Pb zircon geochronology of the Neoproterozoic igneous rocks from Northern Guangxi, South China: Implications for tectonic evolution. Precambrian Res, 2006, 145: 111–130
60 Zhou J C, Wang X L, Qiu J S. Geochronology of Neoproterozoic mafic rocks and sandstones from northeastern Guizhou, South China: Coeval arc magmatism and sedimentation. Precambrian Res, 2009, 170: 27–42
61 Li Z X, Li X H, Kinny P D, et al. Geochronology of Neoproterozoic syn-rift magmatism in the Yangtze Craton, South China and correlations with other continents: Evidence for a mantle superplume that broke up Rodinia. Precambrian Res, 2003, 122: 85–109
62 Wang L J, Griffin W L, Yu J H, et al. Precambrian crustal evolution of the Yangtze Block tracked by detrital zircons from Neoproterozoic sedimentary rocks. Precambrian Res, 2010, 177: 131–144
63 Ling W L, Duan R C, Liu X M, et al. U-Pb dating of detrital zircons from the Wudangshan Group in the South Qinling and its geological significance. Chinese Sci Bull, 2010, 55: 2440–2448
64 Wark D A, Stimac J A. Origin of mantled (rapakivi) feldspars: Experimental evidence of a dissolution and diffusion-controlled mechanism. Contrib Miner Petrol, 1992, 111: 345–361
65 Nekvasil H. Ascent of felsic magmas and formation of rapakivi. Am Miner, 1991, 76: 1279–1290
66 Eklund O, Shebanov A D. The origin of rapakivi texture by sub-isothermal decompression. Precambrian Res, 1999, 95: 129–146
67 Ma C Q, Wang R J. The characteristic and origin of K-feldspar megacrysts in the Zhoukoudian plution, Beijing (in Chinese). Acta Miner Sin, 1990, 10: 323–332
68 Christiansen E H, Haapala I, Hart G L. Are Cenozoic topaz rhyolites the erupted equivalents of Proterozoic rapakivi granites? Examples from the western United States and Finland. Lithos, 2007, 97: 219–246
69 Zhao G C. Palaeoproterozoic assembly of the North China Craton. Geol Mag, 2001, 138: 87–91
70 Zhao G C, Sun M,Wilde S A, et al. Some key issues in reconstructions of Proterozoic supercontinents. J Asian Earth Sci, 2006, 28: 3–19
71 Condie K C. Episodic continental growth models: Afterthoughts and extensions. Tectonophysics, 2000, 322: 153–162
72 Condie K C. Episodic continental growth and supercontinents: a mantle avalanche connection? Earth Planet Sci Lett, 1998, 163: 97–108
73 Condie K C, Des Marais D J, Abbott D. Precambrian superplumes and supercontinents: A record in black shales, carbon isotopes, and paleoclimates? Precambrian Res, 2001, 106: 239–260
74 Liu X M, Gao S, Diwu C R, et al. Precambrian crustal growth of Yangtze Craton as revealed by detrital zircon studies. Am J Sci, 2008, 308: 421–468
75 She Z B. Detrital zircon geochronology of the Upper Proterozic-Mesozoic clastic rocks in the mid-upper Yangtze region (in Chinese). Dissertation for the Doctoral Degree. Wuhan: China University of Geosciences, 2007. 1–131
76 Wang Y B, Liu D Y, Zeng P S, et al. SHRIMP U-Pb geochronology of Xiaotongguanshan quartz-dioritic intrusions in Tongling district and its implications (in Chinese). Acta Petrol Miner, 2004, 23: 298–304
77 Jian P, Zhang Z C, Zhu J P, et al. The Dabie basement older than 2800 Ma: Evidence from the zircon age of granulite from Huangtuling. Acta Geosci Sin, 1997, 18: 65–67
78 Zhou H W, Li X H, Liu Y, et al. Age of granulite from Huangtuling, Dabie Mountain: Pb-Pb dating of garnet by a stepwise dissolution technique. Chinese Sci Bull, 1999, 44: 941–944
79 Wu Y B, Chen D G, Xia Q K, et al. *In-situ* trace element analyses and Pb-Pb dating of zircons in granulite from Huangtuling, Dabieshan by LAM-ICP-MS. Sci China Ser D-Earth Sci, 2003, 46: 1161–1170
80 Xia K Q, Zheng Y F, Ge N J, et al. U-Pb ages and oxygen isotope compositions of zircon from gneiss of Huangtuling, Northern Dabie: Old protolith and multi-stage evolution (in Chinese). Acta Petrol Sin, 2003, 19: 506–512
81 Ling W L. Isotope Geochronology and crustal growth of Proterozoic basement along the northern margin of Yangtze craton: I. Houhe Group and Xixiang Group (in Chinese). Earth Sci-J China Univ Geosci, 1996, 21: 491–494
82 Gao S, Qiu Y M, Ling W L. SHRIMP single zircon U-Pb dating of zircon in Kongling high-grade metamorphic terrain: Evidence for > 3.2 Ga old continental crust in the Yangtze craton (in Chinese). Sci China Ser D-Earth Sci, 2001, 44: 326–335
83 Zhang S B, Zheng Y F, Wu Y B, et al. Zircon isotope evidence for ≥3.5 Ga continental crust in the Yangtze craton of China. Precambrian Res, 2006, 146: 16–34
84 Yu J H, Wang L J, O'Reilly S Y, et al. A Paleoproterozoic orogeny recorded in a long-lived cratonic remnant (Wuyishan terrane), eastern Cathaysia Block, China. Precambrian Res, 2009, 174: 347–363
85 Li X H. Timing of the Cathaysia block formation: Constraints from SHRIMP U-Pb zircon geochronology. Episodes, 1997, 20: 188–192
86 Wan Y S, Liu D Y, Xu M H, et al. SHRIMP U-Pb zircon geochronology and geochemistry of metavolcanic and metasedimentary rocks in Northwestern Fujian, Cathaysia Block, China: Tectonic implications and the need to redefine lithostratigraphic units. Gondwana Res, 2007, 12: 166–183
87 Li Z X, Li X H, Wartho J A, et al. Magmatic and metamorphic events during the early Paleozoic Wuyi-Yunkai Orogeny, southeastern South China: New age constraints and pressure-temperature conditions. GSA Bull, 2010, 122: 772–793